Nature of defect structure in CoO

P. K. Khowash and D. E. Ellis
Department of Physics and Astronomy, Northwestern University, Evanston, Illinois 60201
(Received 19 March 1987)

The defect structure in CoO is examined in an embedded-molecular-cluster model. The point-defect model with isolated vacancies on either metal or oxygen sites is evaluated and compared with more complex defect structures. We calculate the electronic structure of 4:1 interstitial defects and some of their aggregates in CoO. The binding energy is determined to reveal the most stable defect structure, which is the 4:1 tetrahedral complex in this case. Mulliken population analysis and volume integration confirm the formation of a Co^{3+} cation at the tetrahedral site.

I. INTRODUCTION

The nonstoichiometric compound CoO exhibits the rock-salt structure like other transition-metal monoxides. It is understood to behave like a semiconductor, usually p type, and conducts upon doping or by deviation from stoichiometry.[1-3] From the positioning of the "t_{2g}" and "e_g" metal $3d$ subbands with a conventional band-structure calculation,[4-7] CoO is predicted to be metallic, in contrast to the experimental facts. At low temperature, however, with a tetragonal distortion in its antiferromagnetic region, CoO may become an insulator.[8] Most of the physical properties were measured experimentally as a function of temperature and oxygen pressure. Previous analyses focused on effects of point defects, namely metal vacancies with various degrees of ionization.[9-12] The general formula can be written as $Co_{1-x}O$ where x can be varied (0.001 to 0.05) with externally applied partial pressure of O. Dieckmann[9] proposed the point-defect model but later Petot-Ervas *et al.*[13] and Logothetis and Park[14] suggested aggregate cluster defects. Despite extensive investigations, the exact nature of the defect structure is still undetermined.[15-18] Experiments relating to electrical conductivity, cation tracer diffusion, and anion tracer diffusion are in progress to determine the exact nature of defects in this material.

Electronic structure calculations by a molecular-cluster approach are well suited for systems with defects and structural deformation such as vacancies, interstitial and substitutional defects, and local moments. In this work we use the discrete-variational self-consistent-field (DV-SCF) method[19-21] to calculate the charges, density of states, and binding energy for the ideal CoO structure and also defect structures such as the 1:0 single vacancy and 2:1 and 4:1 complexes. Here $m:n$ denotes m octahedral vacancies and n tetrahedral interstitial metal ions. The metal-oxygen distance is varied to get the maximum binding for the ideal case. The binding energies for different vacancies and vacancy-intersitial ratios are also calculated to get insight of the nature of bonding and vacancy stabilization in this compound. The energy separation of the localized $3d$ state from the $2p$ bands is calculated and compared with the experimental photoemission results.[22]

II. METHOD OF CALCULATION

A discrete-variational cluster method[19-21] calculation is carried out to determine the wave functions and eigenvalues of a cluster embedded in the solid. The rest of the solid manifests its presence by providing a crystal field in which the cluster is embedded and thereby minimizing the surface effect to a large extent. Since we have scooped out a cluster from the solid, a potential field is needed to simulate the rest of the solid. This is done by generating a microcrystal surrounding the cluster and placing the atoms at specified lattice positions. In the process of studying defect energies we may introduce charge compensating ions on the lattice. A self-consistent procedure is then employed to generate a Coulomb and exchange-correlation potential field in which the cluster is immersed. Typically, the microcrystal is chosen to extend out to 17–20 a.u., thereby including approximately 250–350 of the surrounding atoms. The matrix elements of the effective Hamiltonian for the one-electron Schrödinger equation are computed as discrete sums rather than as integrals, thus avoiding separate multicenter integrals. The one-electron Schrödinger equation can be written (in Hartree a.u.) as

$$H_\sigma \Psi_{i\sigma}(\mathbf{r}) = \varepsilon_{i\sigma} \Psi_{i\sigma}(\mathbf{r}) , \tag{1}$$

where

$$H_\sigma = [-\tfrac{1}{2}\nabla^2 + V_C(\mathbf{r}) + V_{\mathrm{xc},\sigma}(\bar{r})] , \tag{2}$$

with

$$V_C(\mathbf{r}) = \int \frac{\rho(\mathbf{r}')}{|\mathbf{r}-\mathbf{r}'|} d\mathbf{r}' - \sum_j \frac{Z_j}{|\mathbf{r}-\mathbf{R}_j|} \tag{3}$$

as the Coulomb potential and

$$V_{\mathrm{xc},\sigma}(r) = -3\alpha \left[\frac{3}{8\pi} \rho_\sigma(r) \right]^{1/3} . \tag{4}$$

The simplest Kohn-Sham-Slater exchange potential is chosen here. Also

$$\rho = \rho_{\mathrm{cluster}} + \rho_{\mathrm{crystal}} = \sum_{i,\sigma} f_{i\sigma} | \Psi_{i\sigma}(\mathbf{r}) |^2 + \sum_\nu \rho_{\nu,\mathrm{crystal}} , \tag{5}$$

where $f_{i\sigma}$ are the occupation numbers for the molecular orbitals. The molecular orbital eigenfunctions Ψ^{α} for the α irreducible representation of the point group can be expanded in terms of a basis set of symmetry orbitals where the basis functions are chosen as a linear combination of atomic orbitals–molecular orbital (LCAO-MO) centered on different cluster atomic sites. Finally, the total-energy expression in the local-density approximation is given as

$$E_t = \sum_{\sigma} \left[\sum_i f_{i\sigma}\varepsilon_{i\sigma} - \tfrac{1}{2}\int\int \frac{\rho_\sigma(\bar{\mathbf{r}})\rho_\sigma(\mathbf{r}')}{|\mathbf{r}-\mathbf{r}'|} d\mathbf{r}\, d\mathbf{r}' + \int \rho_\sigma(\mathbf{r})[E_{\mathrm{xc},\sigma}(\mathbf{r}) - V_{\mathrm{xc},\sigma}(\mathbf{r})] d\mathbf{r} \right] + \tfrac{1}{2}\sum_{\alpha}\sum_{\beta}\frac{Z_\alpha Z_\beta}{R_{\alpha\beta}} , \quad (6)$$

where

$$E_{\mathrm{xc},\sigma}(r) = \tfrac{3}{4} V_{\mathrm{xc},\sigma}(\mathbf{r})$$

for the Kohn-Sham potential. The calculated total energies ($\sim 10^5$ eV) are not accurate enough to extract significant differences for the chosen numerical sampling scheme. So a more accurate binding energy may be calculated by a systematic differential scheme[23] $E_b = E_t - E_t^{\mathrm{diss}}$ where E_t^{diss} is the energy of the dissociated ionic system, calculated on the same integration mesh. The dissociation energy (i.e., energy of dissociated atoms or ions) is treated by the spin unrestricted formalism, as in the above equation for the total energy.

The choice of the basis functions plays an important role. In our calculations here, we use minimal atomic-ionic solutions generated on a 300-point radial mesh. A potential well is added to induce bound excited states. The inner radius of the potential well is set at 4 a.u. with the potential-well depth and the cutoff radius being -2.0 and 7.0 a.u., respectively. The value of the Slater exchange parameter α is fixed at 0.7. The orbital functions assigned to different atoms are $1s2s2p$ for the vacancy, [Ar]$3d4s4p4d$ for cobalt and $1s2s2p3s3p$ for oxygen. The $1s$ orbital of oxygen and [Ne]$3p$ orbital for cobalt are treated as core orbitals. A thermal broadening of the occupation numbers $f_{i\sigma}$ of 0.005 H is used to broaden the self-consistent discrete cluster energy levels to get a continuous density of states.

III. RESULTS AND DISCUSSION

A. One-electron energies and charge distribution

CoO is known to be stable at 940 °C in air when decomposed from Co_3O_4.[24] Paidassi *et al.*[25] reported to coexistence of Co_3O_4 and CoO in the temperature range 400–885 °C, but from 905 to 1350 °C only CoO is present. The cubic lattice parameter of the NaCl structure is taken to be 4.26 Å in the composition range $x = 0.001$–0.05.[26]

To study the structural properties of an idealized stoichiometric CoO lattice, we first focus our attention on an eight-atom cluster Co_4O_4 and a larger 27-atom cluster $CoO_6Co_{12}O_8$ embedded in a CoO lattice. A diagonal weighted Mulliken population analysis of the charge density[27,28] reveals orbital occupation numbers and spins for Co and O that closely resemble the chemical values for free ions. The values are presented in Table I for the Co_4O_4 cluster and in Table II for the $CoO_6Co_{12}O_8$ cluster.

TABLE I. Change distribution and spin density for Co_4O_4 cluster in T_d symmetry. Net volume charges (by integration over atomic Wigner-Seitz volumes): Co, 1.12 and O, −1.10. Mulliken populations for charge and spin density.

Co	$3d$	7.10	2.79
	$4s$	0.19	0.04
	$4p$	0.25	0.11
	$4d$	0.06	−0.01
Total		1.38	2.94
O	$2s$	1.83	−0.01
	$2p$	4.56	0.26
	$3s$	0.27	0.19
	$3p$	0.70	0.12
Total		−1.38	0.56

The total density of states obtained by broadening the energy levels with a Lorentzian of 0.4 eV width [Fig. 1(a)] shows an oxygen $2s$ band deep inside the valence band, centered at −21.9 eV. The central band, centered at −9.3 eV, is an admixture of $3d$ Co and $2p$ O. The Co $3d$ contribution grows as we move towards the Fermi level. The multiple humps above the Fermi level are diffuse states due to the hybridization of Co $3d,4p$ and different degrees of O $3s$ and $3p$. This is again clearly seen if the

TABLE II. Charge distribution and spin density for $CoO_6Co_{12}O_8$ cluster in O_h symmetry. Net volume charge (by integration over atomic Wigner-Seitz volumes): Co(1), 1.07; O(1), −0.98; Co(2), 1.24; and O(2), −1.25. Mulliken populations for charge and spin density.

Co(1)	$3d$	6.97	2.91
	$4s$	0.26	0.03
	$4p$	0.04	0.00
	$4d$	0.06	−0.02
Total		1.67	2.93
O(1)	$2s$	1.97	−0.01
	$2p$	5.53	0.13
	$3s$	0.02	0.00
	$3p$	0.19	−0.01
Total		−1.72	0.11
Co(2)	$3d$	6.96	2.95
	$4s$	0.22	0.02
	$4p$	0.02	0.01
	$4d$	0.04	−0.01
Total		1.75	2.97
O(2)	$2s$	1.98	−0.01
	$2p$	5.46	0.11
	$3s$	0.03	−0.00
	$3p$	0.24	−0.01
Total		−1.71	0.11

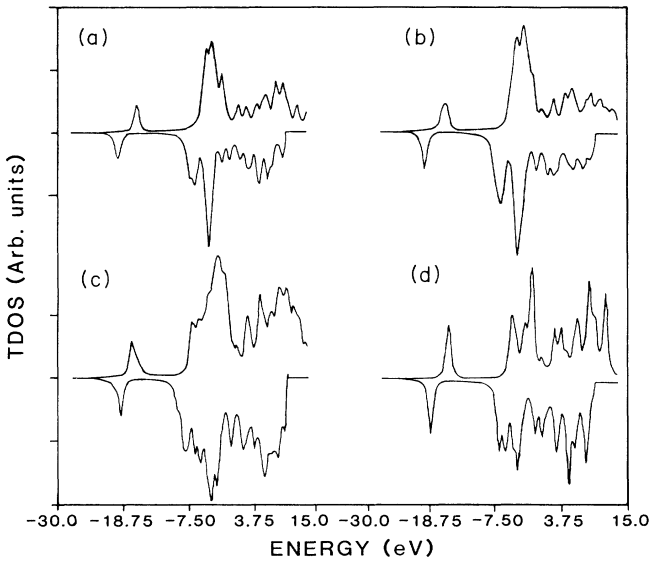

FIG. 1. (a) Total density of states for Co_4O_4 cluster in the self-consistent field. (b) Total density of states for the single vacancy cluster in the self-consistent field. (c) Total density of states for the 2:1 defect cluster in the self-consistent field. (d) Total density of states for the 4:1 defect cluster in the self-consistent field.

TABLE III. Charge distribution and spin density for $VO_6Co_{12}O_8$ vacancy cluser in O_h symmetry (V = vacancy). Net volume charge (by integration over atomic Wigner-Sietz volumes): V, −0.64; O(1), −0.75; Co(1), 0.97; and O(2), −1.31. Mulliken populations for charge and spin density.

V	1s	0.09	-0.01
	2s	0.02	0.00
	2p	0.13	0.02
Total		0.02	0.01
O(1)	2s	1.85	0.00
	2p	4.45	0.41
	3s	0.17	0.02
	3p	0.21	0.01
Total		−0.68	0.44
Co(1)	3d	7.08	2.73
	4s	0.26	0.03
	4p	0.37	0.08
	4d	0.16	−0.02
Total		1.13	2.83
O(2)	2s	1.83	0.00
	2p	4.49	0.05
	3s	0.41	0.08
	3p	1.01	0.09
Total		−1.74	0.22

partial density of states is plotted.

In the Co_4O_4 cluster all the cations are treated identically, each being coordinated to three cluster ligands and three "external" anions. But when we go over to a 27-atom cluster, the central cation, Co(1), is fully coordinated. The ionicities of Co(1) and O(1), as measured by Mulliken populations (Table II), increase as compared to the Co_4O_4 cluster calculation. The central cation has a net spin of 3.1 μ_B. The ionicity of Co(2) turns out to be slightly more than that of Co(1), with the same moment. The experimental magnetic moment per Co ion obtained from neutron diffraction measurements in the ordered state is somewhat larger: $3.4\mu_B$.[29] The total density of states looks similar for both the clusters. The O 2s peak lies approximately −20.8 eV below the Fermi level. The central valence-band peak again is an admixture of O 2p and Co 3d with the percentage of Co 3d contribution increasing as we move toward the Fermi level. The 2p band has an approximate width of 2.4 eV (full width at half maximum) with the peak lying 6 eV below the d-state level. This is in close agreement with the photoemission experiments where the p-band spectrum is about 3 eV wide with the p-d band separation being $\simeq$3–5 eV.[26]

The defect structure of $Co_{1-x}O$ as a function of temperature and oxygen pressure were analyzed using the point-defect model by Dieckmann[9] in his study of electrical conductivity and cation tracer diffusion. The conductivity and thermoelectric power measurements of Logothetis and Park[14] suggest that the major defects are not simple vacancies. Vacancy aggregates are suggested, of which the 4:1 cluster would be one of the favorite candidates. The diffraction studies by Roth[30] in wustite show a similar situation where, apart from the iron vacancies, some ferric ions occupy interstitial tetrahedral sites. Again, a cubic superlattice-generating cluster is observed by Koch and Cohen[31] in their x-ray diffraction work, which identifies the presence of vacancies in nearest-neighbor cation sites surrounding tetrahedral ions. We start with a single vacancy and go over to the 4:1 cluster via the 2:1 defect by systematic removal of Co ions from the cluster. This will lead us to determine from a first-principles model the relative stability of several of the probable defect structures in $Co_{1-x}O$.

The results for a single-vacancy cluster are shown in Table III. V identifies the vacancy, which is seen to gather a small amount of charge. The oxygen atom close to the vacancy is less ionic than the ideal species. The average ionicity of the two types of O is, however, close to that of Co, as demanded by charge neutrality.

The peak deep in the valence band is that of O 2s [Fig. 1(b)]. The O 2p peak is 1.3 eV below the Co 3d peak. In transition-metal oxides with a partially occupied d^n configuration the metal d-s separation gives the band gap. The Co 3d peak and the O 3s peak lie just below and above the Fermi level respectively with an energy separation of $\simeq$4.9 eV. The metal 4s state is 5.3 eV above the O 3s peak. So it is likely that the single-vacancy cluster may behave like a semiconductor.

The volume charge and the Mulliken populations for the charge and spin density for the 2:1 cluster are shown in Table IV. Here Co(1) is the cation at the cube edge and V identifies the vacancy. O(1) and O(2) correspond to oxygen with cations and vacancy as nearest neighbors, respectively, and Co(2) occupies the tetrahedral interstitial

TABLE IV. Charge distribution and spin density for the $Co_2V_2O_4Co$ 2:1 defect cluster in C_{2v} symmetry. Net volume charge (by integration over atomic Wigner-Sietz volumes): Co(1), 0.92; V, −0.56; O(1), −1.16; O(2), −0.83; and Co(2), 1.67. Mulliken populations for charge and spin density.

Co(1)	3*d*	7.28	2.54
	4*s*	0.28	0.08
	4*p*	0.32	0.15
	4*d*	0.14	0.00
Total		0.98	2.77
V	1*s*	0.03	−0.00
	2*s*	0.01	0.00
	2*p*	0.07	0.02
Total		−0.11	0.02
O(1)	2*s*	1.82	−0.00
	2*p*	4.66	0.18
	3*s*	0.28	0.17
	3*p*	0.57	0.12
Total		−1.33	0.47
O(2)	2*s*	1.88	0.00
	2*p*	4.54	0.42
	3*s*	0.11	0.03
	3*p*	0.55	0.11
Total		−1.08	0.56
Co(2)	3*d*	6.49	3.10
	4*s*	0.15	0.01
	4*p*	0.24	0.03
	4*d*	0.45	0.00
Total		1.61	3.14

TABLE V. Charge distribution and spin density for $Co_iV_4O_4$ 4:1 interstitial defect cluster in T_d symmetry. Net volume charge (by integration over atomic Wigner-Sietz volumes): Co, 1.95; V, −0.56; and O, −0.76. Mulliken populations for charge and spin density.

Co	3*d*	6.95	2.84
	4*s*	0.05	0.01
	4*p*	0.19	0.02
	4*d*	0.04	0.03
Total		1.76	2.90
V	1*s*	0.00	−0.04
	2*s*	0.03	0.00
	2*p*	0.11	0.02
Total		−0.13	−0.01
O	2*s*	1.90	0.01
	2*p*	4.57	0.50
	3*s*	0.01	0.01
	3*p*	0.69	0.15
Total		−1.17	0.68

site. The ionicity of Co(2) is almost 1.6 times that of Co(1), about the same ratio expected for 3+ to 2+ formal valency. The ionicity of O(2), close to the vacancy, is less compared to O(1) as expected from the monovacancy results. The vacancy collects a little charge again, about 0.1*e*.

Figure 1(c) shows the total density of states for a 2:1 cluster. The O 2*s* band deep in the valence band is centered at −16 eV. The central band centered around −3 eV is mostly due to Co 3*d* and O 2*p*. The Co 4*s*,4*p* levels combine with O 3*s*,3*p* levels giving rise to multiple peaks above E_F.

Finally, in the 4:1 complex we have a central cation sitting in the center of the cube with four nearest O and four metal vacancies. The resulting populations and charges are shown in Table V. The net spin on the Co is $2.9\mu_B$, slightly larger than at the ideal octahedral site. The vacancy extended wave function V 2*p* picks up more charge compared to the V 1*s* state. This diffuse *p* function is apparently able to provide some of the directional polarization useful in stabilizing the defect.

B. Binding energies

We now look into the binding energy of different clusters. The eight-atom perfect cluster, Co_4O_4, has a binding energy of −13.3 eV per cation-anion pair at the experimental bulk lattice constant, which is comparable to that of the experimental value of −17.5 eV.[32] The metal-oxygen distance when varied predicts the (local) theoretical lattice constant to be 4.16 Å (2–3 % reduced from the experimental value) corresponding to an energy of −14.5 eV (Fig. 2).

To obtain an energetically favorable structure, a detailed study of the geometry of different defect structures is needed. The binding energies calculated here for isolated defects of different shapes and sizes can be intercompared via the binding energy per net number of vacancies.

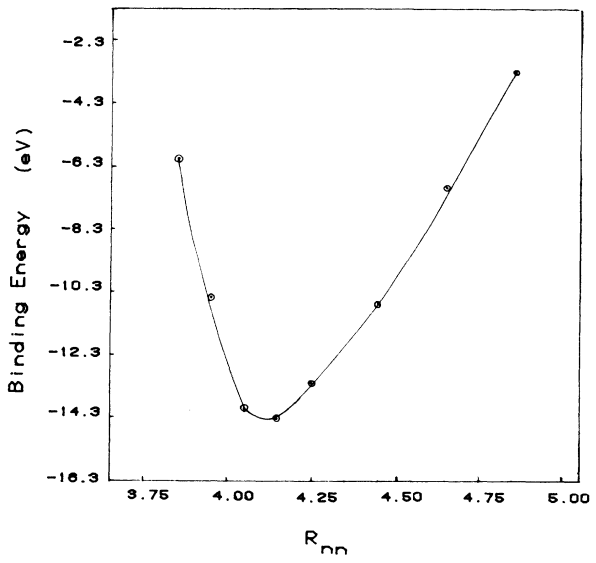

FIG. 2. Binding energy in idealized CoO vs lattice parameter.

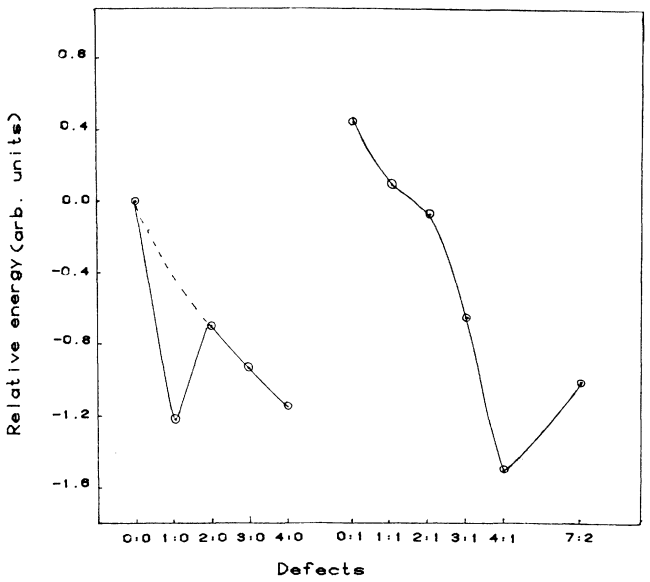

FIG. 3. Relative binding energy per net number of vacancies for various defects of different geometry.

The energies are plotted in relative scale with the ideal Co_4O_4 cluster (no vacancy and no interstitial) as a reference point for vacancies of different order and different vacancy-interstitial ratios. In the process of removing one metal ion after another, we find a dip in energy for the 1:0 cluster, a local minimum (Fig. 3) showing relative stabilization over other vacancies of different order. Other light transition-metal oxides like TiO and VO also show a stable configuration with a single cation vacancy before going over to more complicated ordered structures at particular compositions.[5,33–40] The dip in energy for the 1:0 configuration suggests the reason for success of single-vacancy models used to analyze many experimental results in the past.

Many experiments also indicate that Co^{3+} goes into the tetrahedral site. Our calculated ionicities for Co at a tetrahedral site show an increase as we go from the 2:1 to the 4:1 cluster showing the correct trend. However, the full formal valency is never obtained. When a Co ion is forced into the tetrahedral site of a stoichiometric CoO lattice and the cations from the octahedral sites are removed, we get nonbonding repulsion for the no-vacancy (0:1) and one-vacancy (1:1) cases. The same is the case with one and two oxygen vacancies. The energy decreases slightly for the 2:1 defect but then shows a sudden decrease for the 4:1 cluster as we go through 3:1. The energy of the 4:1 cluster is even lower than the single-vacancy case. This leads us to suppose that with cation vacancy creation under oxygen pressure it is the single vacancy which is first created and then the system evolves to an even more stable 4:1 defect configuration.

An extensive study of the nonstoichiometric $Fe_{1-x}O$ by Press and Ellis[41] using the embedded-cluster approach within the Hartree-Fock-Slater $X\alpha$ formalism show that a tetrahedral "ferric" species in the interstitial site stabilizes the defect structure to a greater degree than any combination of vacancies and octahedral Fe^{3+}. The cluster binding energies indicated greater stability over the simple combinational clusters with a single tetrahredral Fe^{3+}. Of the larger aggregates, the 7:2 (110) cluster exhibited maximum stability. This led us to study the 7:2 (110) cluster of $Co_{1-x}O$. The binding energy is lower than (higher in magnitude) both the single vacancy and the 4:1 configuration. Thus edge sharing of the 4:1 cluster does not appear to be energetically favorable in $Co_{1-x}O$. But the basic mechanism of the formation of defects with M^{2+} octahedral vacancies surrounding a tetrahedral M^{3+} interstitial is found to be similar for $Fe_{1-x}O$ (Refs. 31 and 41–46) and $Co_{1-x}O$. According to the existing literature[46] larger aggregates of the 4:1 cluster in $Co_{1-x}O$ do not show up as in the case of $Fe_{1-x}O$.

IV. CONCLUSIONS

The point-defect model was used initially to analyze experimental data to understand the nature of defect structure in CoO. With further experimentation more complicated defect structures were suggested but the true nature of defect structure is still unresolved. A DV-SCF model was used here to calculate, theoretically, the charges, density of states, and the binding energy for the perfect crystal and certain defect clusters. The magnetic moment of the perfect cluster agrees well with that found from neutron diffraction. Our calculated ionicities for the tetrahedral interstitial Co increase as we go from the 0:1 to 2:1 to the stable 4:1 defect structure. This is in agreement with various experimental interpretations where Co^{3+} is predicted at the interstitial tetrahedral site. The binding energy reveals a local minimum for the 1:0 lattice vacancy indicating how the point-defect model could previously explain some of the experimental results. In examining stability of various defect structures, we find that the 4:1 defect structure has a remarkable dip in energy. Of the larger aggregates, the 7:2 cluster exhibits maximum stability for $Fe_{1-x}O$. Our calculations show no such stability of the 7:2 cluster as compared to the simple isolated clusters with single tetrahedral Co^{3+}. This leads us to suppose that a single vacancy is created first and then the system stabilizes in the 4:1 defect configuration.

ACKNOWLEDGMENTS

This work was supported by the U.S. Department of Energy, under Contract No. DE-FG02-84ER45097. We thank M. R. Press for his contributions to the early stages of this work and for helpful discussions.

[1]J. S. Choi and C. H. Yo, Inorg. Chem. **13**, 1720 (1974).
[2]J. P. Suchet, *Crystal Chemistry and Semiconduction in Transition Metal Binary Compounds* (Academic, New York, 1971), Chap. 6.
[3]P. Kofstad, *Non-Stoichiometry Diffusion and Electrical Conductivity in Binary Metal Oxides* (Wiley-Interscience, New York, 1972), Chap. 11.
[4]L. F. Mattheiss, Phys. Rev. B **5**, 290 (1972).
[5]L. F. Mattheiss, Phys. Rev. B **5**, 306 (1972).
[6]A. P. Malozemoff, A. R. Williams, V. L. Moruzzi, and K. Terakura, Phys. Rev. B **30**, 6565 (1984).
[7]K. Terakura, T. Oguchi, A. R. Williams, and J. Kubler, Phys. Rev. B **30**, 4734 (1984).
[8]D. Adler, in *Solid State Physics*, edited by H. Ehrenreich, F. Seitz, and D. Turnbull (Academic, New York, 1968), Vol. 21.
[9]R. Dieckmann, Z. Phys. Chem. (Neue Folge) **107**, 189 (1977).
[10]B. Fisher and D. S. Tannhauser, J. Chem. Phys. **44**, 1663 (1965).
[11]G. von Schwier, R. Dieckmann, and H. Schmalzried, Ber. Busenges. Phys. Chem. **77**, 402 (1973).
[12]G. von Schwier and H. Schnmalzried, Ber. Busenges. Phys. Chem. **77**, 721 (1973).
[13]G. Petot-Ervas, P. Ochin, and T. O. Mason, in *Transport in Nonstoichiometric Compounds*, Vol. 129 of *NATO Advanced Studies Institute, Series B: Physics*, edited by G. Simkivich and V. S. Stubican (Plenum, New York, 1985), p. 61.
[14]E. M. Logothetis and J. K. Park, Solid State Commun. **43**, 543 (1982).
[15]H. C. Chen and T. O. Mason, J. Am. Ceram. Soc. **64**, C130 (1981).
[16]J. Nowatny, I. Sikova, and M. Rekas, J. Electrochem. Soc. **131**, 94 (1984).
[17]W. K. Chen and N. L. Peterson, J. Phys. Chem. Solids. **41**, 647 (1979).
[18]J. J. Stiglich, D. H. Whitmore, and J. B. Cohen, J. Am. Ceram. Soc. **56**, 211 (1972).
[19]D. E. Ellis and G. S. Painter, Phys. Rev. B **2**, 2887 (1970).
[20]E. J. Baerends, D. E. Ellis, and P. Ros, Chem. Phys. **2**, 41 (1973).
[21]H. Adachi, A. Rosén, and D. E. Ellis, Mol. Phys. **33**, 199 (1977).
[22]D. E. Eastman and J. L. Freeouf, Phys. Rev. Lett. **34**, 395 (1975).
[23]B. Delley and D. E. Ellis, J. Chem. Phys. **76**, 1949 (1982).
[24]T. Ando and R. Umemoto, Osaka Kogyo Gijutsu Shikeusho Kiho **2**, 89 (1951).
[25]J. Paidassi, M. G. Vallee, and P. Pepin, Mem. Sci. Rev. Metall. **62**, 789 (1967).
[26]G. Slack, J. Appl. Phys. **31**, 1571 (1960).
[27]C. Umrigar, D. E. Ellis, D. S. Wang, H. Krakauer, and M. Posternak, Phys. Rev. B **26**, 4935 (1982).
[28]C. Umrigar and D. E. Ellis, Phys. Rev. B **21**, 852 (1980).
[29]D. C. Khan and R. A. Erickson, Phys. Rev. B **1**, 2243 (1970).
[30]W. L. Roth, Acta Crystallogr. **13**, 140 (1960).
[31]F. Koch and J. B. Cohen, Acta Crystallogr. B **25**, 275 (1969).
[32]T. C. Wassington, Adv. Inorg. Chem. Radiochem. **1**, 157 (1959).
[33]J. K. Burdett and T. Hughbanks, J. Am. Chem. Soc. **106**, 3101 (1984).
[34]M. G. Blanchin and L. A. Bursill, Phys. Status Solidi **86**, 491 (1984).
[35]D. Watanbe, O. Terasaki, A. Jotson, and J. R. Castles, J. Phys. Soc. Jpn. **25**, 272 (1968).
[36]J. F. Baumard, D. Panis, and A. M. Anthony, J. Solid State Chem. **20**, 43 (1977).
[37]J. F. Marucco, J. Gautron, and P. Lemasson, J. Phys. Chem. Solids **42**, 363 (1981).
[38]M. G. Blanchin and L. A. Bursill, Phys. Status Solidi A **86**, 101 (1984).
[39]A. Neckel, P. Rostt, R. Eibler, P. Weinberger, and K. Schwarz, J. Phys. C **9**, 579 (1984).
[40]A. L. Ivanovskii, V. A. Gubanov, Yi. G. Zainulin, E. Z. Kurmaev, M. P. Butsman, and B. J. Sborovskii, J. Struct. Chem. (USSR) **23**, 854 (1982).
[41]M. R. Press and D. E. Ellis, Phys. Rev. B **35**, 4438 (1987).
[42]A. K. Cheetham, B. E. F. Fender, and R. I. Taylor, J. Phys. Chem. **4**, 2160 (1971).
[43]C. R. A. Catlow and B. E. F. Fender, J. Phys. C **8**, 3267 (1975).
[44]C. Lebreton and L. W. Hobbs, Radiat. Eff. **74**, 227 (1983).
[45]A. B. Anderson, R. W. Grimes, and A. H. Hener, J. Solid State Chem. **55**, 353 (1984).
[46]R. W. Grimes, A. B. Anderson, and A. H. Hener (private communication).